ELSEVIER

International Journal of Mass Spectrometry 197 (2000) 219–235

International Journal of Mass Spectrometry

Computational and experimental studies of chemical ionization mass spectrometric detection techniques for atmospherically relevant peroxides

Benjamin M. Messer, David E. Stielstra, Christopher D. Cappa, Kurtis W. Scholtens, Matthew J. Elrod*

[a]*Department of Chemistry, Hope College, Holland, MI 49423, USA*

Received 13 April 1999; accepted 9 November 1999

Abstract

We report the results of computational and experimental studies concerning the chemical ionization mass spectrometric detection of hydrogen peroxide (HOOH) and methyl hydroperoxide (CH_3OOH). GAUSSIAN2 (G2) electronic structure calculations are used to predict structures, natural charges of the atoms and energies for the neutral species, as well as for the cation, anion, and the proton and fluoride adduct species. These calculations are used to predict ion–molecule reaction thermodynamics as a guide to the experimental development of chemical ionization mass spectrometric detection methods. Both HOOH and CH_3OOH are predicted to react exothermically with O_2^+ and F^- to yield the cationic and fluoride adduct species, respectively. In addition, CH_3OOH is predicted to react exothermically with H_3O^+ to yield the proton adduct species. The feasibility of F^- chemical ionization mass spectrometric detection of peroxides was experimentally explored through kinetic studies. The fluoride adduct formation reactions for both HOOH and CH_3OOH were found to proceed at or near collision-limited rates. (Int J Mass Spectrom 197 (2000) 219–235) © 2000 Elsevier Science B.V.

Keywords: Chemical ionization; Computational; Thermodynamics; Kinetics; Peroxides

1. Introduction

Hydrogen peroxide (HOOH) is the dominant oxidant in clouds, fogs, or rain in the atmosphere [1]. It is formed from the reaction of two hydroperoxyl radicals

$$HO_2 + HO_2 \rightarrow HOOH + O_2 \quad (1)$$

Methyl hydroperoxide (CH_3OOH) is an important atmospheric species formed by the oxidation of methane in the atmosphere [1]

$$CH_4 + OH \rightarrow CH_3 + H_2O \quad (2)$$

$$CH_3 + O_2 + M \rightarrow CH_3O_2 + M \quad (3)$$

$$CH_3O_2 + HO_2 \rightarrow CH_3OOH + O_2 \quad (4)$$

Under high nitrogen oxide (NO_x) conditions, the following reactions lead to ozone production:

$$CH_3O_2 + NO \rightarrow CH_3O + NO_2 \quad (5)$$

$$NO_2 + h\nu(\lambda < 380\ \text{nm}) \rightarrow NO + O \quad (6)$$

$$O + O_2 + M \rightarrow O_3 + M \quad (7)$$

* Corresponding author. E-mail: elrod@hope.edu

PII S1387-3806(99)00260-2

Recently, Wennberg et al. [2] reported the measurement of higher HO_x levels than predicted in the upper troposphere of the northern hemisphere. Because this result suggests that this region of the atmosphere is not ordinarily dominated by NO_x chemistry, it is therefore more susceptible to anthropogenic NO_x emissions than previously thought. This is an important finding since it indicates that increased air traffic in the upper troposphere may lead to a substantial increase in ozone levels. It was suggested that uncertainties in the reactions that interconvert HO_x and its peroxide reservoirs (such as HOOH and CH_3OOH) might be leading to the underprediction of HO_x levels in the upper troposphere.

The study of reactions involving peroxide chemistry in both the laboratory and the field has been hindered by the analytical detection methods currently available. In laboratory kinetics environments, ultraviolet–visible optical detection methods have traditionally been used, with the difficulty arising from the need to determine temperature-dependent absolute absorption cross sections at wavelengths specific to each peroxide [3]. Because of these problems, there is considerable uncertainty concerning the actual product distribution of reaction (4), with the possibility of a $CH_2O + H_2O + O_2$ channel as the major product pathway. In field detection environments, the most successful analytical method involves the indirect approach of preconcentration of the peroxides, derivatization and fluorescence detection. This method is plagued by sampling artifacts, low sensitivity and poor time resolution [4]. Direct gas phase sampling of CH_3OOH has been tested by using gas chromatography (GC) separation and traditional electron impact mass spectrometry (EIMS) methods, but extensive fragmentation of the CH_3OOH^+ ion ruled out the method for direct use in field studies [5]. Therefore, it is clear that the development of a new analytical technique for the measurement of peroxides would aid in both laboratory and field investigations of atmospheric peroxide chemistry.

EIMS detection methods are widely used in laboratory atmospheric chemistry applications because the approach is much more general than the often molecule-specific optical techniques. However, EIMS sensitivity and selectivity levels are usually inferior to those of the competing optical techniques. The method of chemical ionization mass spectrometry (CIMS) has found increasing use in atmospheric chemistry applications because of its potential for increased selectivity and sensitivity over traditional EIMS methods (which are largely due to the advantages of the ambient ionization conditions typical of CIMS approaches). CIMS has been implemented in laboratory kinetics settings [6,7], as well as in field measurement settings [8–10]. Although the method is, in principle, totally general, chemical ionization schemes (sufficiently fast ion–molecule reactions) must be developed for each chemical species under study. In addition, the complete sample matrix must be evaluated for potential interference reactions that could hinder the proposed chemical ionization scheme.

Although chemical ionization schemes currently exist for the study of many atmospherically relevant species [11], there exists no systematic procedure for the determination of feasible chemical ionization schemes for other species of interest. Currently, chemical ionization schemes are proposed by analogy to similar systems and are empirically tested. We believe that the CIMS method has not been more widely implemented because of this less-than-straightforward developmental aspect of the technique. It is therefore the goal of this article to describe the systematic development of a chemical ionization scheme for use with chemical ionization mass spectrometry, by using the peroxides HOOH and CH_3OOH as specific illustrations of the combined computational/experimental approach.

2. Methodology

In this study, we computationally investigate the four ion–molecule reactions listed below in order to establish the various thermodynamic quantities that are required to evaluate potential chemical ionization schemes:

$$A + e^- \rightarrow A^- \quad (8)$$

$$A + F^- \rightarrow AF^- \quad (9)$$

$$A \rightarrow A^+ + e^- \quad (10)$$

$$A + H^+ \rightarrow AH^+ \quad (11)$$

Processes (8)–(11) can be identified as electron attachment to (8), fluoride adduct formation of (9), ionization of (10), and proton adduct formation of (11) the target species A. In actual practice, process (8) is often achieved via electron transfer reaction from species such as SF_6^- or O_2^-, rather than direct electron attachment, and process (10) is often achieved via electron transfer to species such as O_2^+, which has an unusually large ionization potential. The reaction enthalpies associated with processes (8)–(11) can be identified as the electron affinity (E.A.), fluoride affinity (F.A.), ionization potential (I.P.), and proton affinity (P.A.) of the target species A, respectively. These ion thermodynamic values are either available from the experimental literature, or may be estimated using ab initio calculations. From such ion thermodynamic data, the enthalpy of the chemical ionization reaction may be predicted. For example, NO_2 (2.27 eV) [12] has a higher E.A. than SF_6 (1.05 eV) [13], and thus NO_2 may be ionized with the SF_6^- reagent ion:

$$SF_6^- + NO_2 \rightarrow SF_6 + NO_2^- \qquad \Delta H = -1.22 \text{ eV} \quad (12)$$

Because ion–molecule reactions often proceed near the collision-limited rate, thermodynamic data are often predictive of suitable chemical ionization schemes (i.e. exothermic reactions proceed rapidly) [14]. As much of the relevant ion thermodynamic data is not available for atmospheric species, we first demonstrate the accuracy of high level ab initio calculations in the estimation of these values where experimental information is available. We then apply this computational method to the ion thermodynamics of HOOH and CH_3OOH and establish potential chemical ionization schemes. Finally, a F^- chemical ionization scheme is experimentally tested for two peroxide compounds and found to be well-suited for sensitive detection of these species.

3. Computational

All calculations were performed using the GAUSSIAN94 package [15]. In most cases, accurate energies and geometries for the relevant species were determined using the GAUSSIAN2 (G2) compound method [16]. Recently, the accuracy of the G2 compound method for the determination of ion thermodynamic properties was assessed, and G2 theory was found to be accurate to an average absolute deviation of 0.06 eV for both ionization potentials and electron affinities for the 146 molecules included in the G2 set [17]. We have previously shown that G2 level calculations provide very accurate estimates for neutral and ion thermodynamic values for various atmospherically relevant molecules [18]. The geometries of all species were optimized at the UMP2(full)/6-31G(*d*) level and the vibrational frequencies and zero point energies were obtained from analytical derivatives at the UHF/6-31G(*d*) level. Each stationary point was confirmed as a potential energy minimum by inspection of the calculated frequencies [19]. The G2 method utilizes a series of additive corrections (which include the effects of basis set size and type, and electron correlation) to a base energy calculation at the UMP4/6-311G(*d*,*p*) [20] level in order to simulate a QCISD(T)/6-311+G(3*df*,2*p*) level calculation. For the energy calculations of CH_3OOH^-, the following modifications to the G2 method were necessary to incorporate the effects of the increased diffusivity of the molecular orbitals: (1) doubly diffuse basis sets were substituted into the single point, optimization and frequency calculations used in the G2 method and (2) the ΔE^+ correction was set to zero to prevent the introduction of error due to redundancy. Additional, lower level, energy calculations were carried out for a number of ion–hydrate species at the MP2/6-311G+(*d*,*p*) level of theory (by using the same optimization and vibrational frequency determination steps as used in the full G2 method). Reported natural charges were calculated using Natural Bond Orbital (NBO) Version 3.1 [21] included in the GAUSSIAN94 program package. NBO calculations create an ab initio "Lewis structure" by numerically modeling each species as a collection of atomic hybrids and

bond orbitals [22]. For radical species, the NBO analysis utilizes separate calculations for both the alpha and beta spin electrons, the characteristics of which are then combined to create an overall electronic structure. These "natural" bond orbitals provide insight into the electronic structural changes which occur during the ionization process, and are used to explain observed differences in structure between the neutral and ionic species. All calculations were performed on a Silicon Graphics Indigo2 R4400 workstation.

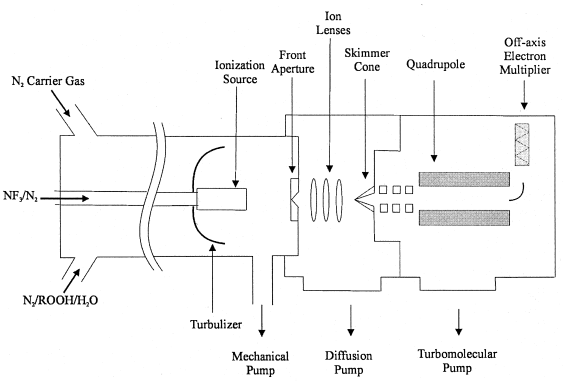

Fig. 1. Experimental apparatus.

4. Experimental

4.1. Synthesis of methyl hydroperoxide

Methyl hydroperoxide is not commercially available; however, O'Sullivan et al. have detailed a straightforward synthesis [23] which was modified here to avoid a potentially dangerous purification step. A mixture of water (14 mL), 30% hydrogen peroxide (4.0 mL), and dimethyl sulfate (1.9 mL), under continuous stirring at 0 °C, was treated with dropwise addition of 40% potassium hydroxide (15 mL). The solution was then slowly heated to 50 °C over a period of 30 min, and the temperature was maintained for another 30 min to drive the reaction to completion. The desired product was collected by slowly bubbling argon gas through the solution, and trapping the escaping vapor in a collection trap containing 25 mL water at 0 °C. In this way, CH_3OOH was collected and CH_3OOCH_3, the other product of the synthesis, was not. The product was positively identified by IR spectroscopy, with characteristic absorbance peaks at 2960 and 1320 cm^{-1} [24]. The product was stored in aqueous solution at 5 °C.

4.2. Mass spectrometric detection

All mass spectrometric measurements for this study were conducted utilizing the chemical ionization mass spectrometer apparatus depicted in Fig. 1. A negative ion chemical ionization scheme (F^-) was used to detect HOOH and CH_3OOH. F^- was produced in a polonium-210 alpha emitting ionization source by passing a large N_2 flow (10 STP L min^{-1}) and 1.0 STP mL min^{-1} of NF_3 through the ionization source. The commercial ionization source consisted of a hollow cylindrical (69 mm length by 12.7 mm diam) aluminum body coated with 10 mCi of polonium-210 on the interior walls. Ions were detected with a quadrupole mass spectrometer housed in a two-stage differentially pumped vacuum chamber. Flow tube gases (neutrals and ions) were drawn into the front chamber through a 0.1 mm aperture, which was held at a potential of −210 V. The ions were focused by three lenses constructed from 3.8 cm i.d., 4.8 cm o.d aluminum gaskets. The front chamber was pumped by a 6 in. 2400 L s^{-1} diffusion pump. The gases entered the rear chamber through a skimmer cone with a 1.0 mm orifice (held at −130 V) that was placed approximately 5 cm from the front aperture. The rear chamber was pumped by a 250 L s^{-1} turbomolecular pump. Once the ions passed through the skimmer cone, they were mass filtered and detected with a quadrupole mass spectrometer.

4.3. Sample standardization, introduction, and mass spectral acquisition

The peroxide samples were standardized by chemical titration using the I_3^- method described by Klassen et al. [25]. The HOOH solutions used were prepared by serially diluting 1 mL of 30% HOOH with distilled water to a final 0.1% HOOH solution.

About 5.0 STP mL min^{-1} N_2 was passed through a bubbler containing ~5 mL of the HOOH solution. This gas phase mixture was then injected into the apparatus and added to a large flow to N_2. The gas phase concentration of HOOH was calculated using the Henry's law coefficient for the 0.1% HOOH solution (as calculated from O'Sullivan et al. [23]), the fractional flow rate of N_2 through the bubbler and the total pressure. Concentrations of about 1×10^{12} molecule cm^{-3} were used to collect mass spectra. The CH_3OOH solution was used as prepared and introduced to the system (and concentrations were calculated) in a manner analogous to HOOH. It should be noted that water vapor ($\sim 1 \times 10^{14}$ molecule cm^{-3}) was also introduced to the system through the use of the bubbler method.

4.4. Ion–molecule kinetics

In order to estimate the rate constant for the reaction of F^- with HOOH and CH_3OOH, fixed distance ion–molecule kinetics studies were performed in a manner similar to previous work by Huey et al. [11]. All measurements were performed at 298 K and 100 Torr, and turbulent flow conditions were maintained. Previous work by Seeley et al. [26] has demonstrated that the turbulent flow experimental conditions of the experiments performed here result in fast mixing of reactant gases such that homogeneous mixing is complete within a few cm of the reactant introduction port. The measurements were performed using pseudo first order conditions ([neutral] $\gg$ [ion]) and the product ion signal was monitored as a function of neutral concentration. The apparatus was tested on the $SF_6^- + NO_2$ reaction, and it was found that the measurements resulted in a systematically lower rate constant (by a factor of about 2) than was previously reported in the literature [11]. As discussed by Adams et al. [27], systematic errors in the measurement of ion–molecule rate constants can occur when the plasma velocity is not matched to the neutral gas velocity. Therefore, in order to eliminate systematic errors in the determination of bimolecular rate constants in our apparatus, relative rate measurements were conducted. The well-studied reaction [28] of $F^- + Cl_2$ was used as the reference for the HOOH and $CH_3OOH + F^-$ kinetics studies. For most experiments, the mean gas velocity was held constant at around 960 cm s^{-1} over a reaction distance of 7.25 cm, yielding a reaction time of 7.6 ms.

5. Results and discussion

5.1. Validation calculations

In order to assess the accuracy of the computational ion thermodynamics method used in this study, several benchmark calculations were performed at various levels of theory for O_2, NO_2, H_2O, and HCl. These calculations were chosen because of the existence of accurate experimental ion thermodynamic data for each of the atmospheric species and because each neutral is experimentally known to affect one of the processes (8)–(11). The results of these calculations are compiled in Table 1. It may be seen that all calculated ion thermodynamic values of interest are not in good agreement with the experimental values for calculations at levels of theory lower than the MP4/6-311+G(d,p) level. Furthermore, the relatively high quantitative accuracy desired in this study (0.1 eV) is not consistently achieved for calculations at a lower level of theory than that of the G2 compound method. For the anions, it is clear that the use of diffuse orbitals (indicated by the "+" notation in the basis set description) is more important than the use of high level electron correlation, which may be noted by comparing the much better quantitative accuracy of the calculations at the MP2/6-311+G(d,p) level compared to those at the MP4/6-311G(d,p) level. The exothermicity of the majority of ion–molecule reaction schemes is on the order of 1 eV, indicating that the 0.1 eV accuracy achieved by the G2 method is sufficient for evaluating most proposed reactions.

As an additional verification of the computationally estimated thermodynamic properties used, the standard enthalpy of formation of CH_3OOH was calculated through the use of the following isodesmic ("equal bond") reaction, in which the number and

Table 1
Ionic standard thermodynamic properties (eV) for selected atmospheric species

	HF/6-31G(*d*)	MP2/6-31G(*d*)	MP4/6-311G(*d*,*p*)[a]	MP2/6-311+G(*d*,*p*)[a]	MP4/6-311+G(*d*,*p*)[a]	G2[a]	Expt.
I.P. (O_2)	12.41	11.55	11.61	11.51	11.69	12.17	12.06[b]
E.A. (NO_2)	0.95	1.03	1.00	1.89	1.87	2.34	2.27[c]
P.A. (H_2O)	7.20	7.20	7.40	7.10	7.14	7.07	7.16[d]
F.A. (HCl)	4.04	4.09	3.77	2.52	2.44	2.54	2.53[d]

[a] Geometry optimized at the MP2/6-31G(*d*) level.
[b] See [46].
[c] See [12].
[d] See [36].

type of bonds in the reactants and products is conserved

$$CH_3OH + HO_2 \rightarrow CH_3OOH + OH \quad (13)$$

By calculating the ab initio enthalpy of reaction (ΔH_r°), the enthalpy of formation (ΔH_f°) can be calculated using the known values of ΔH_f° for CH_3OH, HO_2, and OH. The accuracy of this technique is due to the cancellation of errors affected by maintaining an identical number and type of bonds in the products and reactants. G2 ab initio calculations yielded a ΔH_r° for reaction (13) of 23.2 kcal mol^{-1}. Using literature values [3] of ΔH_f° for CH_3OH, (-3.6 kcal mol^{-1}) HO_2, (2.8 kcal mol^{-1}) and OH (9.3 kcal mol^{-1}), the ΔH_f° of CH_3OOH was found to be -31.5 kcal mol^{-1}. This is in excellent agreement with the literature value [3] of -31.3 kcal mol^{-1}, and serves as an additional verification of the thermochemical accuracy of the G2 ab initio calculations described here.

The energies, equilibrium geometries and natural atomic charges of hydrogen peroxide and methyl hydroperoxide, as well as those of the positive, negative, proton adduct, and fluoride adduct ions, are included in Tables 2–6. For two of the three thermodynamic quantities for which experimental values are known (the ionization potential of O_2 and the proton affinity of HO_2), it is apparent that the G2 level theory is necessary to achieve accurate results. Schematic representations of the geometry of both neutral and ionic species are shown in Fig. 2.

5.2. HOOH and CH_3OOH: structures and natural charges

The equilibrium geometries of HOOH (Table 3) and CH_3OOH (Table 4) are both in good agreement with previous computational work [29,30]. In addition, the HOOH parameters are in good agreement with experimental results ($r_{O–O}$ = 1.475 Å, $r_{O–H}$ = 0.950 Å, ∠OOH = 94.8°, ∠HOOH = 111.5°) [31]. Of particular interest are the O–O and O–H bond lengths and the peroxide dihedral angle, as these parameters are sensitive to changes in the electronic configuration of the molecules. As can be seen in Tables 3 and 4, each of these parameters is nearly identical in both species, with the hydroperoxide functional group remaining relatively unchanged by the methyl substitution. The natural charge analysis for HOOH and CH_3OOH are presented in Tables 5 and 6, respectively, and suggest that the methyl substituent is more electron withdrawing than the hydrogen substituent, as expected.

5.3. $HOOH^-$ and CH_3OOH^-: structures and natural charges

Interestingly, the geometry of $HOOH^-$ is found to be significantly different than neutral HOOH (Table 3), whereas the geometry of CH_3OOH^- is found to differ very little from neutral CH_3OOH (Table 4). The structural differences between neutral HOOH and $HOOH^-$ can be explained by examining the NBO

Table 2
Ionic standard thermodynamic properties (eV) for peroxides and peroxide-related species

	HF/6-31G(*d*)	MP2/6-31G(*d*)	MP4/6-311G(*d*,*p*)[a]	MP2/6-311+G(*d*,*p*)[a]	MP4/6-311+G(*d*,*p*)[a]	G2[a]	Expt.
E.A. (HOOH)	−0.88	−0.85	−0.55	0.43	0.50	0.82	
I.P. (HOOH)	9.46	9.79	9.96	10.19	10.37	10.70	10.58[c]
F.A. (HOOH)	2.38	2.88	2.51	1.62	1.61	1.65	
P.A. (HOOH)	6.97	6.86	6.76	6.84	6.92	6.85	6.99[d]
P.A. (HOO)	6.37	7.09	7.20	7.12	7.04	6.65	6.84[d]
E.A. (CH_3OOH)[b]	−0.88	−0.43		−0.87	−0.84	−0.38	
I.P. (CH_3OOH)	8.53	6.29	9.32	9.59	9.51	9.86	
F.A. (CH_3OOH)	2.33	2.78	2.54	1.57	1.56	1.59	
P.A. (CH_3OOH)	7.38	7.22	7.48	7.20	7.31	7.25	
P.A. (CH_3OO)	7.31	7.59	7.82	7.68	7.68	7.42	

[a] Geometry optimized at the MP2/6-31G(*d*) level.
[b] Geometry optimized at the MP2/6-31++G(*d*) level and all energies calculated with doubly diffuse basis sets for CH_3OOH^-.
[c] See [35].
[d] See [36].

description of the bonding in anion species. In the NBO analysis of the $HOOH^-$ species, the alpha electron interpretation is best described as a complex of an RO radical with an OH^- anion, while the beta electron interpretation indicates a bonding character similar to the neutral species (i.e. with an intact O–O bond). The resulting structure then represents a compromise between the remaining covalent bonding character in the O–O bond and the orientation dependent electrostatic forces between the RO and OH^- subunits. Indeed, the weakened covalent bonding in the HOOH anion (as described by the beta electron interpretation) is manifested in the very large O–O bond length (2.25 Å) calculated for $HOOH^-$. In addition, the charge–dipole forces (as described by the alpha electron interpretation) favor hydrogen

Table 3
MP2/6-31G(*d*) geometric parameters of HOOH and relevant ions

	HOOH	$HOOH^-$	$HOOH^+$	$HOOH_2^+$	$HOOHF^-$
Bond length (Å)					
H_1–O_2	0.976	0.976	1.007	0.999	1.022
O_2–O_3	1.468	2.247	1.351	1.463	1.497
O_3–H_4	0.976	0.976	1.007	0.991	1.022
O_2–H_5 or H_1–F_5				0.999	1.536
Bond angles (deg)					
H_1–O_2–O_3	98.7	56.8	102.3	103.5	92.5
O_2–O_3–H_4	98.7	56.8	102.3	99.7	92.5
H_1–O_2–H_5 or O_2–H_1–F_5				109.4	146.3
Dihedral angles (deg)					
H_1–O_2–O_3–H_4	121.2	227.1	180.0	122.9	0.0
H_5–O_2–O_3–H_4 or O_3–O_2–H_1–F_5				237.1	0.0

Table 4
MP2/6-31G(*d*) geometric parameters of CH_3OOH and relevant ions

	CH_3OOH	CH_3OOH^-	CH_3OOH^+	$CH_3OOH_2^+$	CH_3OOHF^-
Bond length (Å)					
C_1–H_2	1.092	1.097	1.085	1.094	1.100
C_1–H_3	1.094	1.095	1.089	1.089	1.092
C_1–H_4	1.093	1.095	1.088	1.089	1.101
C_1–O_5	1.420	1.428	1.469	1.445	1.410
O_5–O_6	1.470	1.470	1.272	1.492	1.476
O_6–H_7	0.977	0.990	0.990	0.998	1.213
O_6–H_8 or H_7–F_8				0.998	1.160
Bond angles (deg)					
H_2–C_1–H_3	110.3	109.5	112.7	110.8	110.7
H_2–C_1–H_4	110.1	110.7	112.8	110.8	109.1
H_2–C_1–O_5	104.2	104.3	102.3	99.7	106.3
C_1–O_5–O_6	104.5	106.1	111.1	106.6	104.2
O_5–O_6–H_7	98.4	100.6	105.7	102.7	99.1
O_5–O_6–H_8 or O_6–H_7–F_8				102.7	173.4
Dihedral angles (deg)					
O_6–O_5–C_1–H_2	177.4	177.0	177.8	180.0	183.4
O_6–O_5–C_1–H_3	296.3	294.9	243.3	296.7	303.3
O_6–O_5–C_1–H_4	59.0	57.8	58.7	63.2	64.7
H_7–O_6–O_5–C_1	124.0	82.7	179.8	123.7	65.6
H_8–O_6–O_5–C_1 or F_8–H_7–O_6–O_5				236.3	299.9

bonding between the neutral OH radical and OH^- and are manifested by the unusually acute ∠HOO bond angles (56.8°) calculated for $HOOH^-$. This interpretation is in agreement with previous calculations by Hrusak et al., who characterize $HOOH^-$ as a stable intermediate on the reaction pathway between $HOOH + e^-$ and the more thermodynamically stable $O^-{\cdot}H_2O$ [32]. Such significant structural changes for CH_3OOH^- are not observed. Apparently, the additional steric constraints imposed by the methyl substituent prevent the alpha electron interaction from playing a significant role in determining the equilibrium structure of CH_3OOH^-.

Table 5
MP4/6-311+G(*d*,*p*) natural charges of HOOH and relevant ions

Atom	HOOH	$HOOH^-$	$HOOH^+$	$HOOH_2^+$	$HOOHF^-$
H_1	0.495	0.434	0.581	0.588	0.518
O_2	−0.495	−0.934	−0.081	−0.437	−0.583
O_3	−0.495	−0.934	−0.081	−0.272	−0.573
H_4	0.495	0.434	0.581	0.533	0.508
H_5 or F_5				0.588	−0.871

5.4. Electron affinities

The electron affinity of HOOH was determined to be 0.82 eV at the G2 level. Using the previous lower level calculations of Hrusak et al. for various $HOOH^-$ species [32] and the experimental bond dissociation energy for HOOH of 50.5 kcal/mol [33], an electron affinity value of 0.88 eV is obtained for HOOH, which is in good agreement with the results of this study. The electron affinity of CH_3OOH was calcu-

Table 6
MP4/6-311+G(*d*,*p*) natural charges of CH_3OOH and relevant ions

Atom	CH_3OOH	CH_3OOH^-	CH_3OOH^+	$CH_3OOH_2^+$	CH_3OOHF^-
C_1	−0.098	−0.231	−0.283	−0.126	−0.101
H_2	0.153	0.125	0.272	0.220	0.099
H_3	0.136	0.113	0.274	0.191	0.163
H_4	0.146	0.131	0.273	0.191	0.100
O_5	−0.324	−0.651	0.140	−0.160	−0.426
O_6	−0.471	−0.820	−0.255	−0.472	−0.592
H_7	0.458	0.334	0.579	0.578	0.531
H_8 or F_8				0.578	−0.773

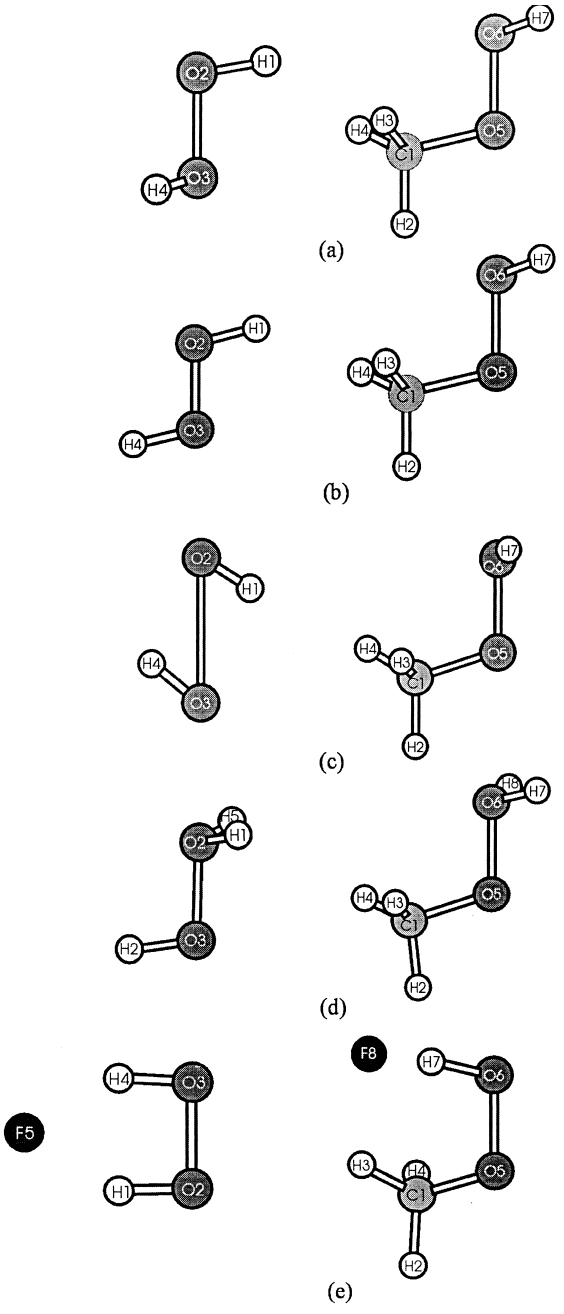

Fig. 2. Schematic representations of (a) HOOH and CH_3OOH, (b) $HOOH^+$ and CH_3OOH^+, (c) $HOOH^-$ and CH_3OOH^-, (d) $HOOH_2^+$ and $CH_3OOH_2^+$, (e) F^-·HOOH and CH_3OO^-·HF.

lated to be −0.38 eV at the G2 level, indicating that the anion is thermodynamically unstable relative to the neutral species and an electron. This instability is most likely the result of the significantly different bonding that is operative in CH_3OOH^- as described in the preceding paragraph. Although CH_3OOH^- is thermodynamically unstable, several fragmentation reactions are possible which could yield thermodynamically stable species. However, we calculate that even the most energetically favorable of these processes is still endothermic:

$$CH_3OOH + e^- \rightarrow CH_3O + OH^- \qquad \Delta H = 0.12 \text{ eV} \qquad (14)$$

5.5. $HOOH^+$ and CH_3OOH^+: structures and natural charges

The peroxide bond in $HOOH^+$ was found to be 0.1 Å shorter than that of HOOH. Similarly, the peroxide bond of CH_3OOH^+ was found to be 0.2 Å shorter than that of CH_3OOH. Additionally, both species were found to shift from a nonplanar structure (∠ROOH = 120°) to a planar geometry (∠ROOH = 180°) upon removal of an electron. This change in geometry is explained by comparing the NBO analyses of the cation and the neutral species; in both ROOH species, the removal of an electron results in a decrease in occupancy of the lone pairs on oxygen. The NBO analysis indicates a change in the calculated hybridization on the oxygen atoms from $sp^{3.0}$ for the neutral to $sp^{2.5}$ for the cation, which is manifested in the sp^2-like planar value of 180° for the peroxide dihedral angle.

5.6. Ionization potentials

The MP2/6-31G(*d*) level calculation for $HOOH^+$ used by the G2 method for geometry optimization has been previously shown to lead to an artifact in the calculation of the antisymmetric fundamental stretch frequency [34]. However, as the frequencies used in the G2 method are calculated at the HF/6-31G(*d*) level (which does not exhibit the same artifact as the MP2 level calculation) the G2 enthalpies are not directly affected by this artifact. Indeed, a comparison of the G2 and experimental I.P. for HOOH (10.58 eV)

[35] indicates that the G2 results are quite accurate for $HOOH^+$. The G2 I.P. for CH_3OOH was determined to be 9.86 eV. Additionally, the G2 enthalpy of $HOOH^+$ and CH_3OOH^+ can be compared to those for HO_2 and CH_3O_2 to yield a calculated proton affinity of HO_2 and CH_3O_2, respectively. The calculated P.A. of HO_2 was found to be 6.65 eV, which is also in good agreement with the experimental value of 6.84 eV [36]. The calculated P.A. of CH_3O_2 was found to be 7.42 eV.

5.7. $HOOH_2^+$ and $CH_3OOH_2^+$: structures and natural charges

The results indicate that the addition of a proton to each species is predicted to occur at the terminal oxygen atom, leading to two chemically identical hydrogen atoms from both the structural and natural charge point of view. Except for a lessened negative natural charge on the terminal oxygen atoms in $HOOH_2^+$ and $CH_3OOH_2^+$, these species are very similar to their neutral parent species.

5.8. Proton affinities

The calculated P.A. of HOOH was found to be 6.85 eV at the G2 level, which is in good agreement with the experimental value of 6.99 eV [36]. The calculated P.A. of CH_3OOH was found to be 7.25 eV at the G2 level.

5.9. F^-·HOOH and CH_3OO^-·HF: structures and natural charges

The most unusual change in geometry of the various ionization products can be seen in the fluoride adducts of HOOH and CH_3OOH. In each case, the resulting product cyclized to form either a five or six membered ring (see Fig. 2), respectively. This cyclization significantly adds to the stability of the fluoride adduct, as calculations which held the peroxide geometry fixed and optimized only the position of the fluoride anion yielded fluoride affinities 0.2–0.3 eV lower than those in which all degrees of freedom are optimized. Because of the chemical symmetry of HOOH, the F^-·HOOH ion forms a symmetrical pentagonal structure in which the electron density of the fluoride ion is shared evenly between the two hydrogen atoms (thus the notation F^-·H_2O_2 would actually more accurately represent the structure of the adduct). In the CH_3OOH case, the chemical symmetry is broken, and the resulting fluoride adduct more closely resembles that of an ROO^- anion complexed with HF. The natural charge analysis and calculated bond lengths for CH_3OOH are consistent with this interpretation, as the terminal oxygen of the peroxide functional group possesses a stronger negative charge than the central oxygen atom and the H–F bond length is more similar to that of the HF molecule than that in the F^-·HOOH ion.

5.10. Fluoride affinities

The calculated fluoride affinities of HOOH and CH_3OOH are 1.65 and 1.59 eV, respectively. In order to further investigate the interesting ring formation observed in the fluoride adducts of HOOH and CH_3OOH and to determine if fluoride adduct formation might be a general chemical ionization scheme for ROOH species, additional calculations were performed on CH_3CH_2OOH. In this case, the MP2/6-31G(*d*) level geometry optimization found that a seven membered ring was the minimum energy structure, indicating that ring formation seems to be general trend for the fluoride adducts of small ROOH species. The calculation of G2-level fluoride affinities was not possible with the available computational resources, but a MP4/6-311+G(*d*,*p*) level fluoride affinity for CH_3CH_2OOH was determined and found to be very close to the value (1.67 eV) calculated with the same level of theory for CH_3OOH. Therefore, we estimate that the fluoride affinities for CH_3CH_2OOH and CH_3OOH are essentially identical.

5.11. Evaluation of potential CIMS detection schemes

The small electron affinity of HOOH and the negative electron affinity of CH_3OOH essentially rule out the use of electron transfer as a possible chemical ionization scheme for these species. The E.A. of

HOOH (0.82 eV) is calculated to be lower than that of SF_6 (1.05 eV [37]), thus eliminating SF_6^- (which is generally a very versatile reagent ion) as a possible ionizing agent. The calculated E.A. of HOOH is higher than the E.A. of O_2 (0.45 eV [38]), indicating that O_2^- could be used as a possible ionizing agent for HOOH. However, we are not aware of any experimental observation of the $HOOH^-$ anion.

The ionization potentials of both HOOH (10.58 eV) and CH_3OOH (10.41 eV) are less than the experimental ionization potential of oxygen (12.063 eV) [39], indicating that both species could be detected by chemical ionization with O_2^+:

$$HOOH + O_2^+ \rightarrow HOOH^+ + O_2 \qquad \Delta H = -1.48 \text{ eV} \tag{15}$$

$$CH_3OOH + O_2^+ \rightarrow CH_3OOH^+ + O_2 \qquad \Delta H = -1.65 \text{ eV} \tag{16}$$

The calculated proton affinity of HO_2 (6.65 eV) is less than the experimental proton affinity of water (7.16 eV) [36], thus ruling out the use of the H_3O^+ reagent ion as a chemical ionization scheme for HO_2. However, the calculated proton affinity of CH_3O_2 (7.42 eV) is higher than that of water, indicating that CH_3O_2 could be detected by using chemical ionization with the H_3O^+ reagent ion:

$$CH_3O_2 + H_3O^+ \rightarrow CH_3OOH^+ + H_2O \qquad \Delta H = -0.26 \text{ eV} \tag{17}$$

In fact, the preliminary findings from this work were the basis for the chemical ionization scheme recently employed by our group in our kinetic study of the neutral CH_3O_2 + NO reaction [40].

As for the RO_2 species, the calculated proton affinity of HOOH (6.85 eV) is less than experimental proton affinity of water (7.16 eV), but the calculated proton affinity for CH_3OOH (7.25 eV) is greater than that of water, suggesting that CH_3OOH could be detected using chemical ionization with the H_3O^+ reagent ion:

$$CH_3OOH + H_3O^+ \rightarrow CH_3OOH_2^+ + H_2O \qquad \Delta H = -0.09 \text{ eV} \tag{18}$$

The fluoride affinities of all three peroxide species are less than the experimental value of the fluoride affinity of SF_5 (1.657 eV [11]), indicating that a fluoride transfer from SF_6^- to the target peroxide species is not exothermic. However, all three species are expected to react exothermically with the fluoride anion, indicating that all three species could be detected by chemical ionization with the F^- reagent ion:

$$HOOH + F^- \rightarrow F^-\cdot HOOH \qquad \Delta H = -1.65 \text{ eV} \tag{19}$$

$$CH_3OOH + F^- \rightarrow CH_3OO^-\cdot HF \qquad \Delta H = -1.59 \text{ eV} \tag{20}$$

$$CH_3CH_2OOH + F^- \rightarrow CH_3CH_2OO^-\cdot HF \qquad \Delta H \approx -1.6 \text{ eV} \tag{21}$$

Although the calculated F.A. of hydrogen peroxide is potentially greater, within the error of the calculations, than the experimental fluoride affinity of SF_5, and could possibly be detected via fluoride transfer with SF_6^-, the reaction with F^- is a general detection method for peroxides. Because fluoride adduct formation results in a significant reduction in entropy (in contrast to the other chemical ionization schemes in which the numbers of reactants and products are the same), we have calculated the free energy change in order to be certain that the fluoride adduct reactions are in fact spontaneous. For example, the calculated free energy change for reaction (19) was found to be −1.34 eV, indicating that enthalpy effects do indeed dominate the free energy change for these reactions.

5.12. Effect of fluoride hydrate formation on the feasibility of fluoride adduct chemical ionization schemes

The formation of fluoride hydrates $[F^-(H_2O)_n)]$ is often unavoidable in the experimental production of

Table 7
Standard enthalpy, entropy and free energy changes at the MP2/6-311+G(d,p) level for fluoride hydrate reactions

	ΔH (eV)	ΔS (eV/K)	ΔG (eV)
$F^- + HOOH \rightarrow HOOHF^-$	−1.65	−0.001 055	−1.34
$F^-(H_2O) + HOOH \rightarrow HOOHF^- + H_2O$	−0.44	−0.000 096	−0.41
$F^-(H_2O) + HOOH \rightarrow HOOHF^-(H_2O)$	−1.12	−0.001 261	−0.75
$F^-(H_2O)_2 + HOOH \rightarrow HOOHF^-(H_2O) + H_2O$	−0.37	−0.000 059	−0.35
$F^-(H_2O)_2 + HOOH \rightarrow HOOHF^-(H_2O)_2$	−0.96	−0.001 305	−0.57
$F^-(H_2O)_3 + HOOH \rightarrow HOOHF^-(H_2O)_2 + H_2O$	−0.32	0.000 264	−0.40

fluoride ions (particularly at atmospheric pressure). Therefore, it is of interest to determine if the fluoride adduct reactions are thermodynamically feasible for reactions with fluoride hydrates as well with the bare fluoride ion. Because the results of the fluoride affinity calculations at the MP2/6-311G+(d,p) level were found to be comparable to those at the G2 level, we calculated the enthalpy and free energy changes for several reactions involving fluoride hydrates and HOOH by using the MP2/6-311G+(d,p) energies of structures optimized at the MP2/6-31G(d) level and HF/6-31G(d) frequencies to calculate the relevant thermodynamic values. In Table 7, we list the reactions considered [those involving $F^-(H_2O)_n$ reactants ranging from $n = 0$ to 3] and the enthalpy, entropy, and free energy changes associated with those reactions. As would be expected, for the reactions in which HOOH is simply exchanged for a water molecule, the enthalpy change is on the order of the difference in the fluoride affinities of HOOH (1.65 eV) and H_2O (1.14 eV [41]), or about −0.5 eV. For the reactions in which HOOH simply adds to the fluoride hydrate complex, the enthalpy change is a significant fraction of the fluoride affinity of HOOH; for example, the $F^-(H_2O) + HOOH \rightarrow F^-(H_2O)HOOH$ reaction enthalpy is calculated to be −1.12 eV. Although this second class of reactions leads to a net reduction in entropy, the free energy change is still found to be more negative than for the exchange reactions. In any case, we find that although the exoergicities of the fluoride adduct reactions involving HOOH and fluoride hydrate reactants are reduced relative those involving the bare fluoride ion, these reactions are nonetheless expected to be thermodynamically feasible and thus potentially useful in chemical ionization applications.

5.13. Experimental results for fluoride adduct formation chemical ionization scheme

In order to verify the proposed chemical ionization schemes (19) and (20), HOOH and CH_3OOH were experimentally detected using the F^- reagent ion. Figs. 3 and 4 are representative mass spectra for relatively high peroxide concentrations ($\sim 1.0 \times 10^{12}$ molecule cm^{-3}). The spectra are most easily interpreted by noting that the reagent ion F^- is actually present in hydrated form [$F^-\cdot(H_2O)_n$], as discussed in the preceding paragraph. Figs. 3 and 4 show that most of the ion signal is contained in the $n = 3$ and 4 hydrates. This hydrate formation occurs despite the very low water concentrations (high purity gases were used and good vacuum was maintained) present in the

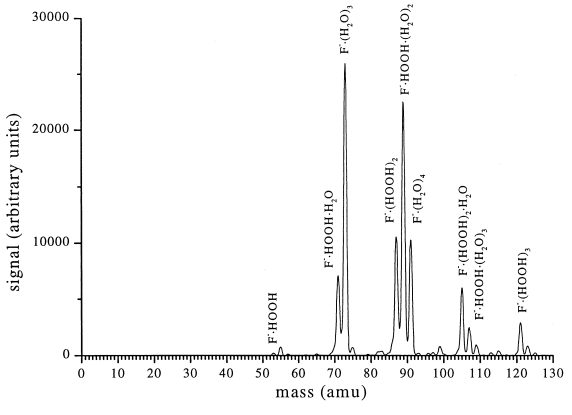

Fig. 3. $F^-(H_2O)_n$ chemical ionization mass spectrum for HOOH.

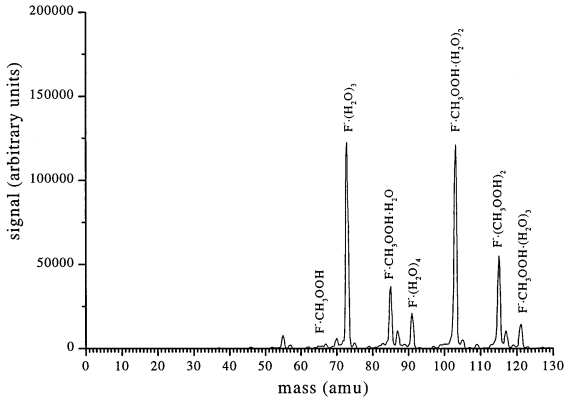

Fig. 4. $F^-(H_2O)_n$ chemical ionization mass spectrum for CH_3OOH.

system. Therefore, the ROOH product ions are also present in hydrated form: $F^-\cdot ROOH\cdot(H_2O)_n$. Figs. 3 and 4 show that the most significant ion signal is contained in the $n = 2$ and 3 hydrates. Therefore, since it appears that one of the hydrated water molecules is lost in the reaction between $F^-\cdot(H_2O)_n$ and ROOH, the dominant reaction pathway seems to be the water exchange reaction described previously:

$$F^-\cdot(H_2O)_n + ROOH \rightarrow F^-\cdot ROOH(H_2O)_{n-1} + H_2O \quad (22)$$

It was a somewhat surprising finding that the additional water ($\sim 1 \times 10^{14}$ molecule cm^{-3}) added from the ROOH sample introduction had little effect on the observed hydrate distribution ($n = 4$ remained the predominant hydrate). Thermodynamic considerations do not serve to explain any unusual stability in the $n = 4$ hydrate [42]. In order to investigate this effect, we added a large amount of additional water vapor ($\sim 2 \times 10^{17}$ molecule cm^{-3}) to the system. Under these conditions, the maximum in the hydrate distribution did shift towards larger hydrates ($n = 6$ was the largest observed hydrate), but again the effect was less than expected from thermodynamic considerations. We propose two possible explanations for the relative insensitivity of the fluoride hydrate distribution to added water vapor. It is possible that the ion sampling potentials on the front aperture and the skimmer cone are great enough to cause some dissociation of the larger hydrates, so that the ions that are transmitted to the quadrupole mass filter are not representative of the ions formed in the reactor. We attempted to investigate this effect, but were not able to obtain ion signals for front aperture potentials of less than −130 V (the distribution did not change in the range from −130 to −210 V). A second explanation rests on the details of the kinetics of the fluoride hydrate formation itself. Although thermodynamic measurements do not indicate any special stability for the $n = 4$ hydrate, it is possible that there is a kinetic bottleneck in the formation of the $n = 5$ hydrate, such that the hydrate distribution is relatively insensitive to water concentration. In any case, this effect is fortuitous because it allows the ion signal to stay relatively concentrated in the $n \leq 4$ hydrates and makes the measurement relatively insensitive to changing water vapor concentrations (which may be encountered in laboratory or field applications of the technique).

5.14. Ion–molecule kinetics

In order to address the ultimate sensitivity of this method for both laboratory kinetic and field detection purposes, the rates of the fluoride adduct formation reactions were estimated. The rate of the relevant ion–molecule reaction is one of the factors that directly determine the ultimate sensitivity of the CIMS method since technical limitations usually require relatively short ion–molecule reactions times.

Unlike selected ion flow tube (SIFT) techniques, which isolate a single *m/z* carrier for kinetic studies, our technique does not allow a separate study of the rates of each of the individual fluoride adduct hydrates with Cl_2, HOOH and CH_3OOH. In addition, because of interferences at the ion reactant *m/z* ratios, the signals resulting from the formation of product ions were followed. Therefore, our kinetic studies represent a weighted average of the relative rates of all processes that lead to a particular product ion. Previous SIFT studies of the $Cl_2 + F^-\cdot(H_2O)_n$ reactions have indicated that there is relatively little dependence of the rate constant on hydration levels of $n < 4$ [28]. Therefore, we must assume that our measurements of the relative rates for reactions involving several

$F^-\cdot(H_2O)_n$ species will not be substantially affected by our monitoring procedure. For the Cl_2, HOOH, and CH_3OOH kinetic studies, we therefore simply chose to follow the largest product ion signal. The following reactions were studied:

$$Cl_2 + F^-\cdot(H_2O)_n \rightarrow F^-\cdot Cl_2 + nH_2O \quad (23)$$

$$HOOH + F^-\cdot(H_2O)_n \rightarrow F^-\cdot HOOH(H_2O)_2 + (n - 2)\,H_2O \quad (24)$$

$$CH_3OOH + F^-\cdot(H_2O)_n \rightarrow CH_3OO^-\cdot HF\,(H_2O)_2 + (n-2)\,H_2O \quad (25)$$

Therefore, the reactions involving Cl_2, HOOH, and CH_3OOH were monitored at *m/z* ratios of 89, 89, and 103, respectively.

The relevant rate equation for the bimolecular ion–molecule reactions is given as

$$\frac{d[\text{product ion}]}{dt} = k[\text{molecule}][\text{reagent ion}] \quad (26)$$

Because the kinetics measurements were performed under pseudo-first-order conditions ([molecule] ≫ [ion]), the rate equation simplifies to

$$\frac{d[\text{product ion}]}{dt} = k'[\text{reagent ion}] \quad (27)$$

(were $k' = k[\text{molecule}]$), and the integrated rate law in terms of the original bimolecular rate constant k is

$$[\text{product ion}] = [\text{reagent ion}]_0 \times (1 - e^{-k[\text{molecule}]t}) + C \quad (28)$$

where C is a constant of integration. For reasons of convenience, we choose to replace $[\text{reagent ion}]_0$ with $[\text{product ion}]_{\text{final}}$. These two quantities are related by the proportionality factor A (A is equal to unity for a reaction which possesses a single reaction channel and has reached completion). If we further relate both concentrations explicitly to the appropriate mass spectrometer signal, Eq. (28) becomes

$$[\text{product ion signal}] = A \times [\text{product ion signal}]_{\text{final}} \times (1 - e^{-k[\text{molecule}]t}) + C \quad (29)$$

The ion–molecule bimolecular rate constant is obtained by measuring the product ion signal as a function of the molecule concentration (for a fixed reaction time). In order to directly compare kinetic runs performed with different molecule concentrations and reaction times, we define the relative time as follows:

$$t_{\text{rel}} = [\text{molecule}]t \quad (30)$$

If the signal is also defined on a relative basis (calculated by dividing $[\text{product ion signal}]_t$ by $[\text{product ion signal}]_{t\,=\,\text{final}}$; the relative signal thus takes on values from 0 to 1) for each kinetic run, plots of relative signal vs. relative time for experiments with different conditions (different detection sensitivities and different reaction times and molecule concentrations) may be directly compared as Eq. (29) simplifies to

$$[\text{relative product ion signal}] = A \times (1 - e^{-kt_{\text{rel}}}) + C \quad (31)$$

Although the constant (C), which originates from the integration of the rate law, is rigorously zero according to the boundary conditions, we retain it as a fitting parameter to account for background signal.

In summary, the basic experiment and data analysis method is as follows: the ROOH ion product signal [i.e. $F^-\cdot ROOH\,(H_2O)_2$] is followed as a function of ROOH concentration. Each relative product signal data point is calculated by dividing each absolute product signal data point by the product signal at the highest molecule concentration ([signal $F^-\cdot ROOH\,(H_2O)_2]_{\text{final}}$). The relative reaction time (t_{rel}) for each data point is calculated from the absolute reaction time (reaction distance/flow velocity) and the molecule concentration for each data point via Eq. (30). The relative product signal as a function of t_{rel} is then fitted via nonlinear least squares techniques to Eq. (31), with A, k, C as adjustable parameters. The process is repeated for the reference reaction (Cl_2 +

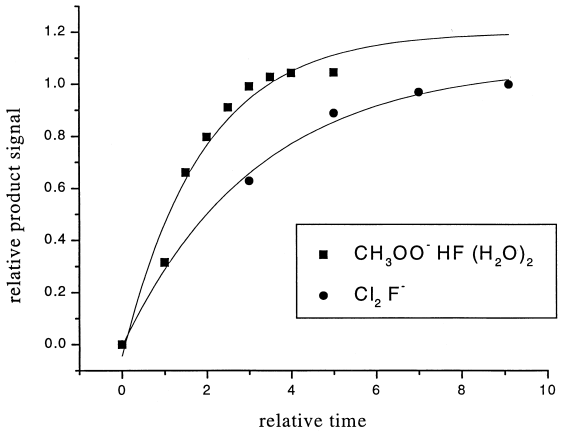

Fig. 5. Relative rate kinetics plot for $F^-(H_2O)_n + CH_3OOH$.

$F^-\cdot(H_2O)_n \rightarrow F^-\cdot Cl_2 + n\ H_2O$) by following $F^-\cdot Cl_2$ as function of [Cl_2] with the data analyzed via the same nonlinear least squares analysis method described previously for the ROOH data. As discussed in the experimental section, the absolute rate constants obtained from our apparatus are systematically low, so we use the ratio of the values of k determined from the fitting process (k_{ROOH}/k_{Cl_2}) to determine relative rate constants instead.

In Fig. 5 we present plots of relative signal versus relative time for experiments involving Cl_2 and CH_3OOH. Because of our definition of the relative signal and relative time, the product rise curves for both the ROOH and Cl_2 experiments may be directly compared on the same graph, despite the fact that different absolute times and molecule concentrations were used. For the data displayed in Fig. 5, comparison of the values of k determined by the nonlinear least squares analysis method indicate that the CH_3OOH reaction is 1.7 times faster than the Cl_2 reaction. We performed several measurements for both the HOOH and CH_3OOH reactions and obtained relative rates of between 1.5 and 3.0 times faster than the analogous Cl_2 reaction for both peroxide species.

We choose to determine approximate absolute rate constants for the ROOH fluoride adduct formation reactions by assuming that the dominant reaction leading to the observed product ion signal involves the $F^-\cdot(H_2O)_3$ species. Although we hope that this choice is not critical [assuming that the ROOH reactions are also characterized by a small variance in the rate constants with hydration values of $n < 4$ as observed for the $Cl_2 + F^-\cdot(H_2O)_n$ reactions], we must choose a specific reaction so that we may compare the rate constant to a specific rate constant for $Cl_2 + F^-\cdot(H_2O)_n$, and so that we may calculate a specific collision-limited rate constant. Seeley et al. determined the rate constant for the $Cl_2 + F^-\cdot(H_2O)_3$ reaction to be 6.4×10^{-10} $cm^3\ s^{-1}$ [28]. Therefore, we estimate the rate constants for both ROOH + $F^-\cdot(H_2O)_3$ reactions are between 9.6 and 19.2×10^{-10} $cm^3\ s^{-1}$.

We calculated the collision-limited rate constants for both HOOH and ROOH with $F^-\cdot(H_2O)_3$ by using average dipole orientation (ADO) theory [14]. The electrostatic properties (dipole moment and polarizability) needed in the ADO calculations were obtained from experimental measurements [43,44] for HOOH ($\mu = 1.5728$ D, $\alpha = 2.286$ Å^3) and estimated from MP2/6-311G(d,p) level ab initio calculations for CH_3OOH ($\mu = 1.76$ D, $\alpha = 3.16$ Å^3). The ADO calculations yield collision-limited rate constants of 14.2×10^{-10} and 14.7×10^{-10} $cm^3\ s^{-1}$ for HOOH + $F^-\cdot(H_2O)_3$ and $CH_3OOH + F^-\cdot(H_2O)_3$, respectively. Because our experimental estimates for the rate constants bracket this theoretical upper limit, our results indicate that the fluoride adduct formation reactions for HOOH and CH_3OOH proceed at a rate indistinguishable from the collision-limited rate. Therefore, because the fluoride-adduct formation reactions for HOOH and CH_3OOH are very fast, the CIMS detection sensitivity level for peroxides via this method has the potential to be very high. For our experimental apparatus (which was designed for laboratory neutral kinetics studies and was not exclusively configured for maximum detection sensitivity), we estimate that our sensitivity level for both ROOH species is better than 100 ppt at 100 Torr total pressure.

The process of implementing a chemical ionization detection scheme for a particular chemical environment also involves a consideration of potential interference reactions. Interference reactions usually involve the unwanted reaction of another neutral

molecule present in the chemical system with either the reagent ion or one of the product ions. These reactions have the potential to lower the sensitivity of the method and to create multiple signal carriers for a single *m/z* ratio. For laboratory experiments, where the number of chemical constituents can be controlled, it is relatively straightforward to consider the effect of interference reactions. However, for field experiments, the presence of high concentrations of water vapor and numerous abundant chemical species can make this consideration more difficult. Although the $F^-(H_2O)_n$ chemical ionization schemes presented here for peroxides have a good probability of being useful in laboratory settings [$F^-(H_2O)_n$ methods have previously been successfully implemented in laboratory kinetics studies [40,45], the hydrate formation issue and the reactivity of $F^-(H_2O)_n$ with atmospheric acids may complicate the implementation of this approach in field settings. Indeed, our computational prediction that CH_3OOH should react with H_3O^+ may be a more promising route for the field detection of this compound, as the $H_3O^+(H_2O)_n$ reagent ion is one of the predominant ions formed in ionization sources operating under atmospheric conditions.

6. Conclusions

The equilibrium structures, natural charges and energies for neutral ROOH (R = H, CH_3) species and their cationic, anionic, proton adduct, and fluoride adduct analogs have been calculated via G2 ab initio methods. The anions are found to be either marginally thermodynamically stable or not stable, and therefore are not expected to be useful as chemical ionization products. However, the ionization potentials of both HOOH and CH_3OOH were predicted to be less than that of O_2, suggesting that both species could be detected using chemical ionization mass spectrometric methods and an O_2^+ chemical ionization scheme. The calculated proton affinity of CH_3OOH suggests that this species could be detected with a H_3O^+ chemical ionization scheme. The fluoride adduct analogs of all three ROOH species were predicted to form exothermically via the reaction ROOH + F^-. Each fluoride adduct species was predicted to form a five-, six-, or seven-member intramolecular ring system for R = H, CH_3, and CH_3CH_2, respectively. Computational studies predict that this cyclization increases the stability of the fluorine adduct by 0.2–0.3 eV over F^-·ROOH complexes which were fixed at the neutral ROOH geometry. The fluoride adduct reactions involving fluoride hydrate reactants and ROOH were also calculated to be thermodynamically feasible. The feasibility of the fluoride adduct formation chemical ionization method was experimentally verified for HOOH and CH_3OOH using a chemical ionization mass spectrometer. Unique mass signals were observed at the parent mass and at masses corresponding to hydrated parent ion. The rates of these reactions were found to proceed at or near the collision limited rate, thus making them good candidates for sensitive CIMS applications.

As demonstrated for the case of ROOH, unique chemical ionization schemes can be developed for atmospherically relevant systems through the combined use of computational and experimental studies. Using high level ab initio thermodynamic calculations, the range of possible ionizing agents can be sufficiently narrowed to aid the experimental confirmation and kinetic study of a proposed chemical ionization mass spectrometric detection method. We hope that the procedure described in this work provides a model for a general development method of CIMS detection schemes, and that the applications developed here aid in the study of peroxides in the laboratory and field environments.

Acknowledgements

The authors thank Dr. Nicole Bennett for her assistance with the synthesis of CH_3OOH. The authors acknowledge support from the Camille and Henry Dreyfus Foundation, the American Chemical Society, Petroleum Research Fund, Research Corporation, the Michigan Space Grant Consortium, and the National Science Foundation (ATM-9874752).

References

[1] J.H. Seinfeld, S.N. Pandis, Atmospheric Chemistry and Physics: From Air Pollution to Climate Change, Wiley, New York, 1998.
[2] P.O. Wennberg, T.F. Hanisco, L. Jaegle, D.J. Jacob, E.J. Hintsa, E.J. Lanzendorf, J.G. Anderson, R.-S. Gao, E.R. Keim, S.G. Donnelly, L.A. Del Negro, D.W. Fahey, S.A. McKeen, R.J. Salawitch, C.R. Webster, R.D. May, R.L. Herman, M.H. Proffitt, J.J. Margitan, E.L. Atlas, S.M. Schauffler, F. Flocke, C.T. McElroy, T.P. Bui, Science 279 (1998) 49.
[3] W.B. DeMore, S.P. Sander, D.M. Golden, R.F. Hampson, M.J. Kurylo, C.J. Howard, A.R. Ravishankara, C.E. Kolb, M.J. Molina, Chemical Kinetics and Photochemical Data for Use in Stratospheric Modeling, JPL Publication No. 97-4, Jet Propulsion Laboratory, Pasadena, CA, 1997.
[4] M. Lee, B. Noone, D. O'Sullivan, B.G. Heikes, J. Atmos. Oceanic Technol. 12 (1995) 1060.
[5] J. Polzer, K. Bachman, J. Chromat. A 653 (1993) 283.
[6] P.W. Villata, L. Huey, C.J. Howard, J. Phys. Chem. 99 (1995) 12829.
[7] J.B. Lipson, M.J. Elrod, T.W. Beiderhase, L.T. Molina, M.J. Molina, J. Chem. Soc. Faraday Trans. 93 (1997) 2665.
[8] L.G. Huey, E.J. Dunlea, E.R. Lovejoy, D.R. Hanson, R.B. Norton, F.C. Fehsenfeld, C.J. Howard, J. Geophys. Res. 103 (1998) 3355.
[9] F.L. Eisele, H. Berresheim, Anal. Chem. 64 (1992) 283.
[10] O. Mohler, F. Arnold, J. Atmos. Chem. 13 (1991) 33.
[11] L.G. Huey, D.R. Hanson, C.J. Howard, J. Phys. Chem. 99 (1995) 5001.
[12] K.M. Ervin, J. Ho, W.C. Lineberger, J. Phys. Chem. 92 (1988) 5405.
[13] A.E.S. Miller, T.M. Miller, A.A. Viggiano, R.A. Morris, J.M. Van Doren, S.T. Arnold, J.F. Paulson, J. Chem. Phys. 102 (1995) 8865.
[14] M.T. Bowers, Gas Phase Ion Chemistry, Academic, New York, 1979.
[15] M.J. Frisch, G.W. Trucks, H.B. Schlegel, P.M.W. Gill, B.G. Johnson, M.A. Robb, J.R. Cheeseman, T. Keith, G.A. Petersson, J.A. Montgomery, K. Raghavachari, M.A. Al-Laham, V.G. Zakrzewski, J.V. Ortiz, J.B. Foresman, J. Cioslowski, B.B. Stefanov, A. Nanayakkara, M. Challacombe, C.Y. Peng, P.Y. Ayala, W. Chen, M.W. Wong, J.L. Andres, E.S. Replogle, R. Gomperts, R.L. Martin, D.J. Fox, J.S. Binkley, D.J. Defrees, J. Baker, J.P. Stewart, M. Head-Gordon, C. Gonzalez, J.A. Pople, GAUSSIAN 94 (Revision E.2), Gaussian, Inc., Pittsburgh, PA, 1995.
[16] L.A. Curtiss, K. Raghavachari, G.W. Trucks, J.A. Pople, J. Chem. Phys. 94 (1991) 7221.
[17] L.A. Curtiss, P.C. Redfern, K. Raghavachari, J.A. Pople, J. Chem. Phys. 109 (1998) 42.
[18] B.M. Messer, M.J. Elrod, Chem. Phys. Lett. 301 (1999) 10.
[19] Calculated frequencies for all species are available from the authors upon request.
[20] L.A. Curtiss, J.E. Carpenter, K. Raghavachari, J.A. Pople, J. Chem. Phys. 98 (1993) 1293.
[21] E.D. Glendening, A.E. Reed, J.E. Carpenter, F. Weinhold, NBO Version 3.1.
[22] J.P. Foster, F. Weinhold, J. Am. Chem. Soc. 102 (1980) 7211.
[23] D.W. O'Sullivan, M.L. Lee, B.C. Noone, B.G. Heikes, J. Phys. Chem. 100 (1996) 3241.
[24] G.L. Vaghjiani, A.R. Ravishankara, J. Phys. Chem. 93 (1989) 1948.
[25] N.V. Klassen, D. Machington, H.C.E. McGowan, Anal. Chem. 66 (1994) 2921.
[26] J.V. Seeley, J.T. Jayne, M.J. Molina, Int. J. Chem. Kinet. 25 (1993) 571.
[27] N.G. Adams, M.J. Church, D. Smith, J. Phys. D. 8 (1975) 1409.
[28] J.V. Seeley, R.A. Morris, A.A. Viggiano, J. Phys. Chem. 100 (1996) 15821.
[29] J. Koller, M. Hodoscek, B. Plesnicar, J. Am. Chem. Soc. 112 (1990) 2124.
[30] R.D. Bach, P.Y. Ayala, H.B. Schlegel, J. Am. Chem. Soc. 118 (1996) 12765.
[31] R.H. Hunt, R.A. Leacock, C.W. Peters, K.T. Hecht, J. Chem. Phys. 42 (1965) 1931.
[32] J. Hrusak, H. Frierichs, H. Schwarz, H. Razafinjanahary, H. Chermette, J. Phys. Chem. 100 (1996) 100.
[33] X. Luo, P.R. Fleming, T.R. Rizzo, J. Chem. Phys. 96 (1992) 5659.
[34] J. Hrusak, S. Iwata, J. Chem. Phys. 106 (1997) 4877.
[35] F.S. Ashmore, A.R. Burgess, J. Chem. Soc. Faraday Trans. 2 73 (1977) 1247.
[36] E.P. Hunter, S.G. Lias, J. Phys. Chem. Ref. Data 27 (1998) 413.
[37] E.C.M. Chen, J.R. Wiley, C.F. Batten, W.E. Wentworth, J. Phys. Chem. 98 (1994) 88.
[38] M.J. Travers, D.C. Cowles, G.B. Ellison, Chem. Phys. Lett. 164 (1989) 449.
[39] NIST Standard Reference Database 69, November 1998 Release, NIST Chemistry WebBook (http://webbook.nist.gov/chemistry).
[40] K.W. Scholtens, B.M. Messer, C.D. Cappa, M.J. Elrod, J. Phys. Chem. 103 (1999) 4378.
[41] S.S. Xantheas, L.X. Dang, J. Phys. Chem. 100 (1996) 3989.
[42] R.G. Keesee, A.W. Castleman, J. Phys. Chem. Ref. Data 15 (1986) 1011.
[43] E.A. Cohen, H.M. Pickett, J. Mol. Spectrosc. 87 (1981) 582.
[44] E. Barbagli, M. Maestro, Chem. Phys. Lett. 24 (1974) 567.
[45] J.V. Seeley, R.F. Meads, M.J. Elrod, M.J. Molina, J. Phys. Chem. 100 (1996) 4026.
[46] R.G. Tonkyn, J.W. Winniczek, M.G. White, Chem. Phys. Lett. 164 (1989) 137.